Conformational Rearrangements of Tail-less Complex Polypeptide 1 (TCP-1) Ring Complex (TRiC)-Bound Actin†

Laila Villebeck,‡ Malin Persson,§ Shi-Lu Luan,|| Per Hammarström,§ Mikael Lindgren,⊥ and Bengt-Harald Jonsson*,‡

Divisions of Molecular Biotechnology and Chemistry, IFM, Linköping University, Linköping 58183, Sweden, Department of Clinical Microbiology, Umeå University, 90187 Umeå, Sweden, and Department of Physics, The Norwegian University of Science and Technology, 7491 Trondheim, Norway

Received October 6, 2006; Revised Manuscript Received January 3, 2007

ABSTRACT: The mechanism of chaperonins is still under intense investigation. Earlier studies by others and us on the bacterial chaperonin GroEL points to an active role of chaperonins in unfolding the target protein during initial binding. Here, a natural eukaryotic chaperonin system [tail-less complex polypeptide 1 (TCP-1) ring complex (TRiC) and its target protein actin] was investigated to determine if the active participation of the chaperonin in the folding process is evolutionary-conserved. Using fluorescence resonance energy transfer (FRET) measurements on four distinct doubly fluorescein-labeled variants of actin, we have obtained a fairly detailed map of the structural rearrangements that occur during the TRiC−actin interaction. The results clearly show that TRiC has an active role in rearranging the bound actin molecule. The target is stretched as a consequence of binding to TRiC and further rearranged in a second step as a consequence of ATP binding; i.e., the mechanism of chaperonins is conserved during evolution.

The folding of many proteins in both prokaryotes and eukaryotes is assisted by molecular chaperones, of which one important family consists of the chaperonins. The chaperonins are divided into two groups: Group I chaperonins, present in eubacteria, mitochondria, and chloroplasts, and Group II chaperonins, found in the cytosol of eukaryotes and Archaebacteria. The best studied is the Group I chaperonin GroEL, but a large amount of research has now also been conducted on the eukaryotic chaperonin tail-less complex polypeptide 1 (TCP-1)[1] ring complex (TRiC). All chaperonins are large oligomeric complexes, composed of two identical 7−9-membered rings stacked back to back. Each ring contains a central cavity where unfolded polypeptides (substrates or target proteins) can bind and reach their native structure. Here, we will focus on the details of the structure and mechanism of the eukaryotic cytosolic chaperonin TRiC.

In TRiC, each ring comprises eight different but homologous (30% identity) subunits (*1*−*4*), with molecular masses of 52−65 kDa (*2*). Each subunit consists of three domains: the equatorial domain with the nucleotide-binding site, the apical domain, which is involved in substrate binding, and a central hinge, the intermediate domain, that transfer nucleotide-dependent conformational changes in the equatorial domain to the substrate-binding apical domain. A helix is protruding from the tip of the apical domain of each subunit (*5*). These protrusions point outward in the ADP or nucleotide-free state of TRiC, thus leaving the chaperonin in an open conformation. In this conformation, the substrate-binding sites are exposed and a target protein can bind to the chaperonin cavity (*6*). ATP binding induces conformational changes, leading to downward and inward movement of the apical domains (*6*), which in turn cause a closure of the central cavity (*6*, *7*). Consequently, the target protein is confined inside the chaperonin. It is proposed that TRiC undergoes further conformational changes at ATP hydrolysis (*8*), and the release of the target protein occurs after hydrolysis of ATP (*6*).

In the pioneering studies (*3*, *9*), it was anticipated that the cytoskeletal proteins actin and tubulin were the main targets for TRiC, but the list of proposed target proteins has become longer (*10*). About 10% of newly synthesized proteins in the eukaryotic cell are suggested to interact with TRiC (*11*). Some results indicate that target proteins interact with TRiC in a partly structured, slowly formed quasi-native conformation (*12*−*15*), ready to undergo the final stage in their folding process upon the ATP-dependent action of TRiC.

Despite the knowledge of ATP-dependent conformational changes in the chaperonin, as a consequence of ATP binding and hydrolysis, little is known about how the target protein is affected by these conformational changes. Two general models have been presented to explain the folding activity of chaperonins, the Anfinsen cage model (*16*) and the more active role as an unfoldase (*17*).

† We are grateful for financial support from the NanoMat program of the Norwegian Science Research Council to M.L. and from the Swedish Research Council to B.-H.J.

* To whom correspondence should be addressed. Telephone: +46-13-288935. Fax: +46-13-122587. E-mail: nalle@ifm.liu.se.

‡ Division of Molecular Biotechnology, IFM, Linköping University.

§ Division of Chemistry, IFM, Linköping University.

|| Umeå University.

⊥ The Norwegian University of Science and Technology.

[1] Abbreviations: TRiC, TCP-1 ring complex; TCP-1, tail-less complex polypeptide 1; FRET, fluorescence resonance energy transfer; EPR, electron spin resonance; IPTG, isopropyl-β-D-1-thiogalactopyranoside; GuHCl, guanidium chloride; AMP-PNP, adenylyl imidodiphosphate; 6-IAF, 6-iodoacetamidofluorescein; EDTA, ethylenediaminetetraacetic acid; DTT, dithiothreitol; β-actin^{cys-}, engineered, cysteine-devoid β-actin molecule; β-actin^{cys+}, engineered β-actin containing one or two cysteine residues at selected positions.

10.1021/bi062093o CCC: $37.00
Published on Web 04/07/2007

According to the Anfinsen cage model (*16*), the chaperonin cavity is a passive container, providing a sequestered microenvironment for unfolded target proteins. In contrast, we and others hypothesize that the chaperonin plays an active role in reorganizing the bound protein substrate through unfolding of the misfolded structure. In the Anfinsen cage model, folding or refolding to the native bioactive state is supposed to proceed, while the protein is protected from unfavorable interactions and aggregation in the crowded environment of the cell. However, several experiments have shown that this model is not applicable to all target proteins, because certain proteins are ejected from the cavity with each round of ATP hydrolysis, irrespective of its conformational state (*18*−*23*). In several studies, the binding of the protein Rubisco to GroEL has been used as a model to illuminate possible unfoldase activity of the chaperonin. In support of the more active role in unfolding the bound target, it was proposed that it was the binding of ATP and the co-chaperonin GroES to GroEL that induces a stretching force that acts on the bound substrate, thereby promoting unfolding (*24*). This model was however recently challenged because no effect of ATP−GroES-induced stretching could be detected when the experiments of Shtilerman et al. were revisited (*25*) mainly because of the lack of protected hydrogens in the GroEL-bound state. Importantly, the binding of Rubisco to GroEL in the absence of ATP did support a stretched unfolding mechanism in a fluorescence resonance energy transfer (FRET) study (*26*), which also demonstrated that the binding of ATP and GroES promotes a compaction of the bound substrate rather than stretching (*26*).

We have previously made spectroscopic and thermodynamic studies on the bacterial chaperonin GroEL, where we concluded that conformational changes in the prokaryotic chaperonin force a bound target protein to expand its hydrophobic core. In these studies, electron spin resonance (EPR) spectroscopy was used to detect structural changes of paramagnetic molecular probes attached to cysteine variants of the substrate protein (*27*). This was complemented with studies of fluorescent probes and distance changes detected using FRET (*28*). The unfoldase effects of GroEL were by both of these methods completely independent of ATP and GroES. We also showed that this rearrangement was promoted through conformational changes in GroEL induced by substrate protein binding in the absence of ATP and GroES (*29*). The unfolding that was forced by use of the binding energy was concluded to give the substrate protein a chance to correct a misfolded substructure into the correct one, which in turn leads to an increased yield of native protein (*30*, *31*).

In this work, we show how the structure of actin is affected upon binding to the eukaryotic chaperonin TRiC. Removal of the native cysteine residues in actin afforded two important characteristics of the TRiC substrate: (i) Actin becomes significantly destabilized and hence prone to misfolding and aggregation, which makes the cysteine-devoid actin molecule (β-actin^{cys-}) an excellent substrate for TRiC capture. (ii) The β-actin^{cys-} can be mutated to provide cysteine residues at specific sites for attachment of fluorophores. A series of single and double cysteine variants, denoted β-actin^{cys+}, was designed and labeled with fluorescein molecules, allowing for distance determination using homo-FRET. We report on large dynamical changes in the actin molecule when it binds to a TRiC/ADP complex and its further rearrangements as a consequence of the ATP-dependent conformational changes in TRiC. Non-native β-actin^{cys+} initially adopts a "stretched" conformation upon binding to the chaperonin. The conformational changes in TRiC caused by ATP binding [here mimicked by the ATP analogue, adenylyl imidodiphosphate (AMP-PNP), to avoid hydrolysis] rearrange the bound β-actin^{cys+} molecule that achieves a more native-like structure.

EXPERIMENTAL PROCEDURES

Cloning and Mutagenisis of Actin. The coding region for chicken β-actin, giving a amino acid sequence identical to the bovine β-actin (*32*, *33*), was isolated from a chicken cDNA library and was inserted directly after a T7 promotor into the *Nco*I site of the plasmid pACA (*34*), also containing the BLA gene, which gives ampicillin resistance. The gene was further modified by site-directed mutagenesis. Naturally occurring cysteine residues were replaced by alanine to give a plasmid called pβACTIN. Thereafter, a set of actin variants that contain cysteine at selected positions was generated. Five variants R39C, W86C, Q137C, Q246C, and L261C contain a single cysteine residue, and four variants R39C/Q246C, W86C/L261C, Q137C/L261C, and Q246/L261C contain a pair of cysteine residues. Plasmids containing the correct mutation and otherwise an intact gene sequence were transformed into *Escherichia coli* BL21/DE3 cells.

Expression and Purification of Engineered Actin Variants. *E. coli* BL21/DE3 containing the plasmid harboring the actin variant gene was grown to an OD_{600} of 0.6−0.8 at 37 °C in 2× Luria Bertani medium containing 60 mg/L ampicillin. Protein expression was induced by 0.5 mM isopropyl-β-D-1-thiogalactopyranoside (IPTG), and growth was allowed to proceed at room temperature overnight. The cells were harvested by centrifugation at 4 °C and washed 2 times by resuspending the pelleted bacteria in 100 mL of wash buffer, containing 20 mM Tris-HCl (pH 7.5), 10 mM ethylenediaminetetraacetic acid (EDTA), and 1% Triton X-100, followed by centrifugation at 4400*g* for 20 min at 4 °C. The bacterial cells were ultrasonicated, and the lysate was centrifuged at 14900*g* at 4 °C for 10 min. The pellet, containing inclusion bodies of actin, was resuspended in 25 mL of wash buffer, and a granule of DNase I was added. After this, the inclusion bodies were thoroughly washed by 7 rounds of alternating centrifugation at 14900*g* and resuspension in wash buffer. The washed inclusion bodies were denatured in 8 M guanidium chloride (GuHCl) and 5 mM dithiothreitol (DTT) before loading on a 130 mL Superdex 75 gel-filtration column pre-equilibrated in 4 M GuHCl, 1 mM DTT, and 60 mM Tris-HCl (pH 7.2). The protein was eluted with the same buffer at a flow rate of 0.5 mL/min. The eluted fractions were analyzed on sodium dodecyl sulfate−polyacrylamide gel electrophoresis (SDS−PAGE). The concentration of actin in the samples was determined spectrophotometrically at 290 nm, using $\epsilon_{290} = 0.63$ mL mg^{-1} cm^{-1} (*35*).

Fluorescein Labeling of Engineered Actin Variants. Labeling with fluorescein was done in a solution of 4 M GuHCl and 60 mM Tris-HCl at pH 7.2 containing a 10-fold molar excess of the 6-iodoacetamidofluorescein (6-IAF) reagent over free cysteines. The reaction was allowed to proceed

for 2 h at room temperature, and excess reagent was removed with gel filtration and 2 rounds of dialysis.

The degree of labeling was calculated by determination of free thiol groups at 412 nm, using Ellman's reagent and $\epsilon_{412} = 14\,150\ M^{-1}\ cm^{-1}$ (*36*).

Purification of TRiC. The purification of TRiC is based on the method of Ferreyra and Frydman (*37*) but is considerably modified and simplified, and therefore, we describe the complete purification procedure in the Supporting Information.

Samples for Fluorescence Measurements. Fluorescence measurements were performed in folding buffer on 600 μL samples with 0.4 μM labeled actin and 1.6 μM TRiC, unless otherwise indicated. The final GuHCl concentration was 12−32 mM in the "0 M GuHCl" and the TRiC-containing fluorescence samples.

DTT was added to TRiC to a final concentration of 1 mM, and the sample was incubated at 30 °C for 15 min. Labeled and denatured actin was diluted 125−300-fold, by adding 1 μL at a time, into the TRiC solution. The binding reaction was allowed to occur for 45 min at 30 °C. Insoluble aggregates were removed by centrifugation at 17700*g*.

Steady-state fluorescence anisotropy spectra were recorded on a Hitachi F-4500 spectrofluorometer at 21 °C. The emission intensity was monitored at 524 nm (10 nm slit), and the corresponding excitation spectrum was collected in the region of 460−510 nm (5 nm slit) at the four different polarization configurations: VV, VH, HH, and HV (Figure 3A). After homo-FRET measurements of the actin−TRiC/ADP complex, the sample was split up into two tubes; one was incubated with 160 μM AMP-PNP, and the other was incubated with 1.6 μM DNase I and 160 μM ATP for 60 min. Homo-FRET measurements of denatured β-actin^{cys+} were performed at 7.5 and 4 M GuHCl, containing 60 mM Tris-HCl at pH 7.2, with an actin concentration of 0.4 μM. Control experiments were also conducted on β-actin^{cys+} diluted into folding buffer devoid of TRiC/ADP. Selected samples prepared in the same way as those for steady-state anisotropy measurements were also used for time-resolved measurements. Time-resolved anisotropy decay spectra were recorded using time-correlation single photon counting with an IBH time-resolved spectrometer. As an excitation source, a 469 nm laser diode was used with a time profile < 200 ps [full width at half maximum (fwhm)]. The emission monochromator was set to 525 nm using a 16 nm slit. An apparatus constant G was measured for all samples at 7.5 M GuHCl for the relevant excitation and emission wavelengths (469 and 525 nm, respectively). The average of nine different measurements was used in the analysis ($G = 0.646$). A GG495 filter (Melles Griot) was used to block residual scatter from the excitation source.

Distance Determinations by Use of Steady-State and Time-Resolved Anisotropy and Homo-FRET. The distances were calculated from measurements of energy transfer between the fluorescent probes. The efficiency of such transfer can be detected by measurements of changes in the anisotropy of the fluorescent probes as described by Lakowicz (*38*) and Hamman et al. (*39*). A detailed description of the theoretical background for the measurements of distances is given in the Supporting Information.

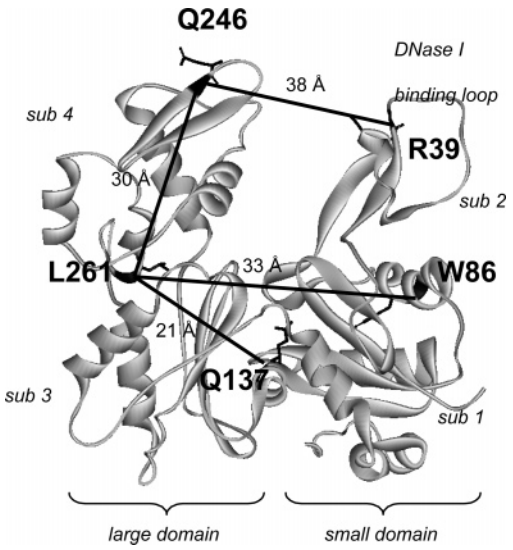

FIGURE 1: Structure of native β-actin and the positions chosen for site-specific labeling. The ribbon representation is based on the crystal structure of bovine β-actin [Protein Data Bank (PDB) accession number 1HLU]. The positions chosen for labeling are marked in black, and the distances between their β carbons are indicated.

RESULTS

Labeling of Actin. To analyze structural rearrangements of the target protein in a functional TRiC chaperonin cycle, homo-FRET measurements were used to detect changes in distances between selected positions in β-actin. It is well-known that actin requires the ATP-dependent action of the chaperonin TRiC to reach its native state in mammalian cells (*13*, *40*), and it was therefore selected as a target protein. The β-actin gene chosen for expression in *E. coli* was from *Gallus gallus* (chicken). β-Actin is a highly conserved protein and shares 100% amino acid identity in chicken, cow, and many other mammalian species, including humans. The choice of a β-actin with an identical amino acid sequence to the bovine β-actin gives us a natural system to explore in this study.

Homo-FRET measurements require the presence of two identical fluorophores attached to the target at predetermined positions. To facilitate the site-specific attachment of the fluorophores, a set of engineered actin variants was generated by site-directed mutagenesis on the designed β-actin^{cys-}, in which six naturally occurring cysteines have been replaced by alanines. Notably, three of the cysteine side chains are located at the surface of the actin molecule and hence probably do not contribute to the stability of the protein. The choice to replace the native cysteine residues by alanine residues was made because only a small number of native interactions are deleted, and therefore, the effects of the mutations on the structure and stability of the actin molecule are minimized. Subsequently, new cysteine residues were introduced, one at the time, at five positions, creating the variants R39C, W86C, Q137C, Q246C, and L261C, each containing one cysteine residue, and R39C/Q246C, W86C/L261C, Q137C/L261C, and Q246C/L261C, each containing two cysteine residues (Figure 1). These β-actin^{cys+} variants were labeled with the fluorophore 6-iodoacetamidofluorescein (hereafter referred to as fluorescein). This fluorescent probe has a small Stoke's shift, giving rise to homo-FRET

where the Förster radius is 40 Å (*39*). This allows the measurement of distances between approximately 20 and 70 Å, depending upon experimental conditions and rotational diffusion of the label, a range suitable for gaining information about structural rearrangements within the actin molecule at different conditions (here, at 7.5, 4, and 0 M GuHCl, bound to TRiC/ADP and to TRiC/AMP-PNP).

The purification of the actin variants resulted in high yields, typically 25 mg of pure protein from 2 L of *E. coli* culture (Figure 2A). The labeling with fluorescein was efficient, leading to more than 90% labeled cysteine residues for all of the variants.

Purification of TRiC. The method for purification of TRiC from bovine testis originates from Ferreyra and Frydman (*37*) but has been considerably simplified. The initial homogenization, ultracentrifugation, and ammonium sulfate precipitation was performed essentially the same as by Ferreyra and Frydman. The subsequent DE52 cellulose and MonoQ chromatography steps were excluded, and instead, 1 mM ATP was added to the sample, which was loaded directly onto HiTrap Heparin columns. The fractions that contained ≥95% pure TRiC (Figure 2B) were pooled for subsequent change of buffer and concentration. The protein was incubated with ADP to obtain the open conformation that can accept the substrate. From this simplified protocol, 22 mg of TRiC is obtained from 250 g of testis in 3 days. A characteristic set of bands corresponding to the molecular weights of the TRiC subunits, 52−65 kDa, is seen on a SDS gel after Commassie staining (Figure 2B). To verify that the purified TRiC complex has the native structure, sedimentation equilibrium analysis by ultracentrifugation was performed. The results (Figure 2C) fit well with a molecular mass of 950 kDa, strongly indicating that the purified TRiC adopts the native quaternary structure with the complete set of 16 subunits.

Distance Determinations by Homo-FRET Reveal Rearrangements in TRiC-Bound Actin. When denatured β-actin^{cys+} is diluted into a folding buffer (conditions that favor the native state) in the absence of the chaperonin, actin molecules that are not able to reach the native state are prone to form aggregates. This was manifested as an increased anisotropy of labeled β-actin^{cys+} in the folding buffer compared to labeled β-actin^{cys+} in 4 M GuHCl (Figure 3F). To suppress the formation of such aggregates, the β-actin^{cys+} variants were diluted into a TRiC-containing folding solution to give a final 4-fold molar excess of TRiC in the actin−TRiC association experiments. The affinity between TRiC and all of the β-actin^{cys+} variants is high, leading to a high degree of binding of all variants, which is important for the interpretation of the distance data from the homo-FRET measurements. The use of excess TRiC in the preparation of the actin−TRiC/ADP complex efficiently hinders the formation of actin aggregates, and the mixing procedure thus gave essentially homogeneous samples of actin−TRiC/ADP complexes, suitable for the homo-FRET measurements.

The homo-FRET phenomenon is manifested as an exchange rate between two fluorophores that results in a drop in fluorescence anisotropy. The reduction of time-resolved or steady-state anisotropy of labeled double variants compared to the anisotropy of the single variants can be used to calculate the distance between two labeled positions in a protein molecule as outlined in detail in the Supporting Information. Time-resolved control measurements were made for denatured β-actin^{cys+} samples as shown in Figure 4. Representative steady-state emission intensity curves for the possible polarization combinations are shown in Figure 3A. Typical steady-state anisotropy excitation spectra on the labeled single and double variants in the presence of TRiC

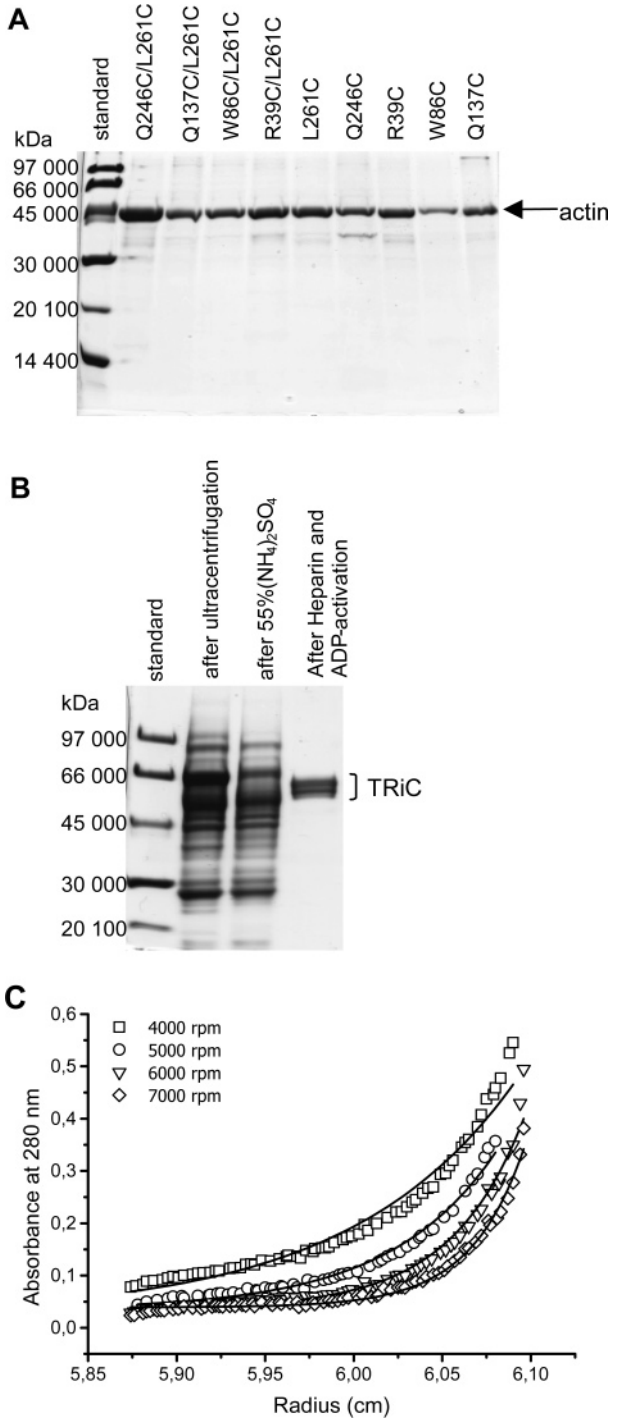

FIGURE 2: High degree of purity for all actin variants and TRiC. (A) SDS gel showing the purity of the actin variants after purification and labeling with fluorescein. (B) SDS gel showing the purity in TRiC samples after ultracentrifugation (lane 2), 55% $(NH_4)_2SO_4$ (lane 3), and Heparin chromatography (lane 4). (C) Sedimentation equilibrium analysis. The TRiC/ADP complex was centrifuged at four speeds. Solid lines show the best fit, according to the self-association model in the Beckman software. The analysis indicates a molecular mass of 950 kDa, showing an intact TRiC complex.

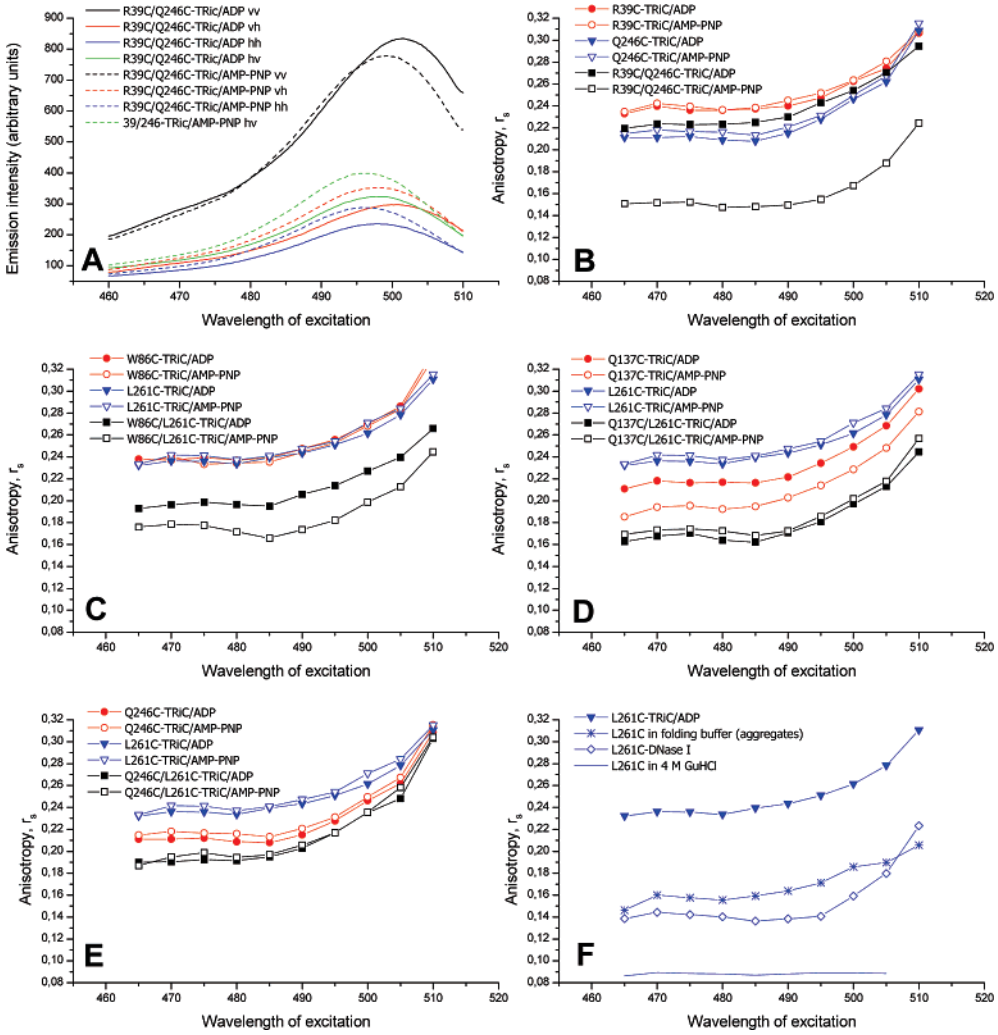

FIGURE 3: Steady-state excitation and anisotropy spectra of actin variants labeled with fluorescein. (A−F) Excitation at 465−510 nm (10 nm slit) and emission at 524 nm (5 nm slit). (A) Steady-state emission spectra for fluorescein-labeled actin bound to TRiC/ADP (—) and TRiC/AMP-PNP (- - -) with the different polarization configurations VV (black), VH (red), HH (blue), and HV (green). (B−E) Steady-state anisotropy spectra for the fluorescein-labeled actin double variants R39C/Q246C (B), W86C/L261C (C), Q137C/L261C (D), and Q246C/L261C (E) with their respective single variants bound to TRiC/ADP (●, ▼, and ■) and TRiC/AMP-PNP (○, ▽, and □). Where homo-FRET is present, the double variants have lower anisotropies than their corresponding single variants. (F) Representative steady-state anisotropy spectra for actin denatured in 4 M GuHCl (—), diluted from 4 M GuHCl into folding buffer (◇), bound to TRiC/ADP (▼), and actin that has gone through one chaperonin cycle (ATP-binding and hydrolysis) leading to the release and binding of DNAse I (*).

with ADP or AMP-PNP are shown in parts B−F of Figure 3. The distances between fluorophores were calculated for all doubly labeled variants in the presence of the denaturant and in the various actin−TRiC complexes (Table 1).

Although the fluorophores are identical in each labeled β-actin^{cys+} single variant, the local environment in terms of the amino acids adjacent to the probe position is different. The anisotropy is dependent upon not only the tumbling of the complex (because of the size) but also the local movement of the fluorophores in the more or less folded conformations. Thus, a β-actin^{cys+} single variant with a fluorescein in a rigid position gives rise to a higher anisotropy than a β-actin^{cys+} single variant where fluorescein has more freedom to reorient. If the contribution to the anisotropy for a fluorescein in one position is different from the contribution from the other position, it is not possible to uniquely determine the distance. Obviously, the use of the average anisotropy from both single variants to determine the distance causes uncertainties in such cases. The uncertainties in distance determination is presented as a distance range (in parenthesis) in Table 1 for each β-actin^{cys+} double variant at all different conditions. This distance range is obtained from the calculation of the distance (R) for each double variant using "r_{01}" for each of the corresponding single variants individually; i.e., the distance is calculated with the ("worst case") assumption that only one of the fluorophores contributes to the anisotropy in the absence of homo-FRET. Thus, the range in a way presents the shortest and longest distances possible between the fluorophores in each double variant.

The anisotropy is dependent upon the tumbling of the complex and the local rotation of a fluorophore. Different positions in the actin molecule have different environments, which in turn affect the mobility of an attached fluorescein molecule. To verify that the steady-state anisotropy really reflected a decrease in anisotropy because of an exchange rate and was not artifacts as a result of changes in anisotropy because of structural differences between the single and double variants, selected samples were also subjected to time-resolved measurements (see the Experimental Procedures and the Supporting Information). It is noteworthy that the slowest

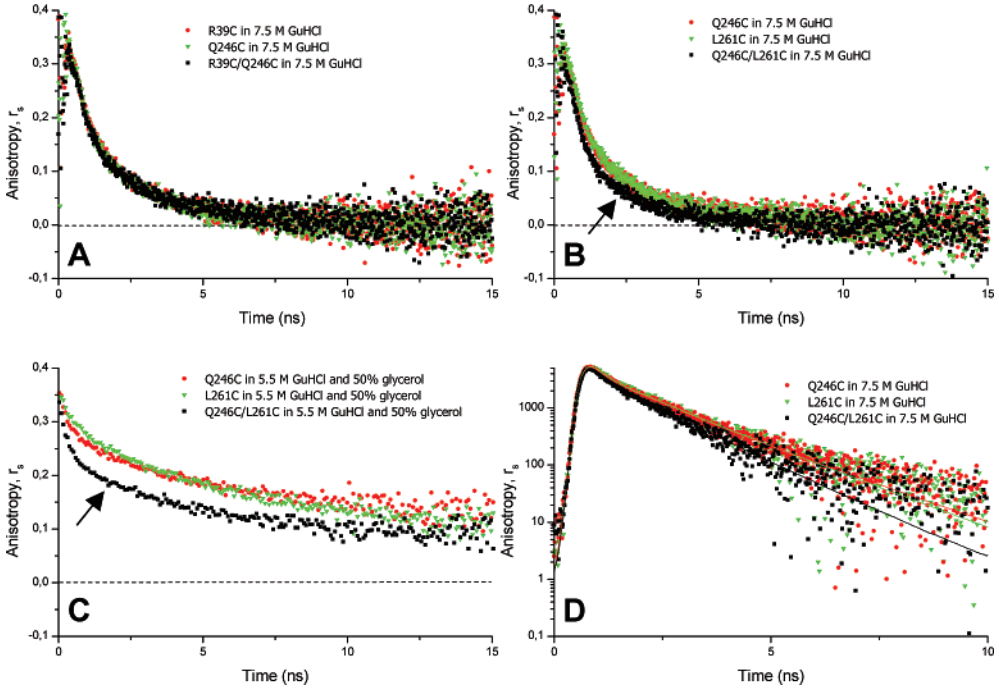

FIGURE 4: Time-resolved anisotropy decay spectra of actin variants labeled with fluorescein in 7.5 M GuHCl and in 5.5 M GuHCl with 50% glycerol. Excitation at 469 nm and emission at 525 nm. (A and B) Time-resolved anisotropy decay spectra (direct fit) for the fluorescein-labeled actin double variants R39C/Q246C (A) and Q246C/L261C (B) with their respective single variants in 7.5 M GuHCl. The arrow in B indicates a faster decay, because of homo-FRET, for the doubly labeled variant (■) where the fluorescein molecules are relatively close in space. This phenomenon is not seen in the R39C/Q246C variant (A), where the fluorescein molecules are far apart. (C) Representative time-resolved anisotropy decay spectra for a fluorescein-labeled actin double variant and the corresponding single variants in 5.5 M GuHCl and 50% glycerol. The arrow indicates a fast decay for the doubly labeled variant (■). The higher viscosity of the 50% glycerol sample makes the homo-FRET the dominating process, thus separating the anisotropy decay of the double variant from the corresponding single variants better than in B. The decay does not decay to 0 because of the higher viscosity of the sample and the short lifetime (3.5−4 ns) of fluorescein. (D) Representative time-resolved anisotropy decay spectra with the impulse reconvolution fit [diff(t)] for doubly and singly fluorescein-labeled actin variants.

Table 1: Conformational Rearrangements of TRiC-Bound Actin[a]

	7.5 M GuHCl		4 M GuHCl	0 M GuHCl	TRiC/ ADP	TRiC/ AMP-PNP	
	steady-state FRET distance (Å)	time-resolved FRET distance (Å)	steady-state FRET distance (Å)	steady-state FRET distance (Å)	steady-state FRET distance (Å)	steady-state FRET distance (Å)	crystal structure distance between β **carbons (Å)**
R39C/ Q246C (sub 2−4)[b]	>55 (59−)	64 (63−65)	56 (52−64)	46 (41−53)	>68 (57−)	35 (33−38)	37
W86C/ L261C (sub 1−4)[b]	>55 (56−)	51 (47−69)	>55 (64−)	41 (37−47)	45 (44−45)	38 (38−39)	33
Q246C/ L261C (sub 4)[b]	45 (44−46)	46 (45−46)	41 (40−42)	49 (42−58)	47 (44−53)	47 (44−52)	29
Q137C/ L261C (sub 1−4)[b]	47 (45−48)	45 (44−46)	47 (44−52)	32 (31−33)	39 (37−41)	42 (38−48)	20

[a] Values in parenthesis represent the distance range appearing when the r_{01} values of the individual actin variants are used separately, one at a time (see the Experimental Procedures). [b] Indicates the subdomains of actin that harbor the fluorophore.

component of rotational diffusion of the denatured labeled variants in 7.5 M GuHCl is very similar for all of the single variants (Table 2 in the Supporting Information and parts A and B of Figure 4). The slow component has the most impact on the time-integrated or average (steady-state) anisotropy. Thus, the fast reorientation of the "local structure" at each probe site can be expected to give only a small contribution to the calculated distance.

In Table 1, some distances are given as lower limits (e.g., >55 Å for denatured actin monomers). When the distance between the probes is large, the difference in anisotropy between the single and double variants is too small to resolve in steady-state experiments. Because the calculated distance depends upon several parameters, this lower limit was estimated for each case based on both the uncertainty in anisotropy and the absolute anisotropy value for the actual Förster distance (see the Supporting Information and the Experimental Procedures for details). It can be concluded that the upper range by which we can estimate the distances is approximately 70 Å for TRiC-bound actin using the

steady-state data for slowly tumbling complexes, i.e., the β-actin^{cys+}−TRiC complex. This is in agreement with Hamman et al. (*39*). The rotational dynamics at the probe site is crucial for the distance measurements. When the viscosity of the solute is increased, the motion of the flourophores becomes slower and, consequently, the rotational diffusion relaxing the apparent anisotropy will be reduced, which gives rise to larger anisotropy values. To simulate the slow tumbling of the β-actin^{cys+}−TRiC complex, denatured actin was mixed with glycerol, resulting in samples containing 0.4 μM actin, 5.5 M GuHCl, and 50% glycerol. The glycerol increases the viscosity of the sample, thus slowing down the tumbling. Hereby, in the apparent anisotropy, the energy transfer becomes the dominating process and the anisotropy decay of the double variant is much faster than that for any of the single variants (Figure 4C). This viscosity effect was observed for all doubly labeled variants (data not shown).

The homo-FRET in terms of fluorescence anisotropy was used to determine the structural changes in the β-actin^{cys+} molecule at different unfolding conditions, after binding to TRiC to form an β-actin^{cys+}−TRiC/ADP complex, and finally to monitor how the nucleotide-dependent conformational changes in TRiC affect the structure of the bound β-actin^{cys+} molecule. First, as a control of the steady-state homo-FRET measurements, distances in all β-actin^{cys+} double variants were examined in 7.5 M GuHCl with both the steady-state and time-resolved techniques. A comparison between distance values determined by steady-state and time-resolved measurements show that the steady-state method is applicable for measuring distances in this system (Table 1 and the Supporting Information). Second, the β-actin^{cys+} variants were diluted into folding buffer devoid of TRiC/ADP. Here, actin is prone to aggregate, as can be seen by an increase in the anisotropy as a result of slower tumbling of a larger complex, as previously mentioned. Overall, the results indicate that the actin molecule becomes more compact as the denaturant is removed (Table 1). However, because the distribution of aggregated states of actin at 0 M GuHCl is not well-characterized, the 4 M GuHCl distance determinations are chosen as the reference state in the distance comparison between non-native and TRiC-bound actins in the following discussions. Nevertheless, the results from the 0 M GuHCl measurements importantly show that the possible presence of a small fraction of non-native actin (as a monomer or in soluble aggregates) in the actin−TRiC/ADP samples does not contribute to the observed chaperonin stretching effect discussed below.

Third, the binding of β-actin^{cys+} to the open, ADP-bound state of TRiC was analyzed. As β-actin^{cys+} is diluted from 4 M GuHCl to the TRiC-containing folding solution, a stable β-actin^{cys+}−TRiC/ADP complex is formed. After the formation of this complex, the distance between 39 (in the tip of subdomain 2) and 246 (in the tip of subdomain 4) is increased by $\geq$12 Å, while the distance between 86 and 261 is shortened by $\geq$10 Å, compared to the non-native state in 4 M GuHCl. The changes between the positions in the other two variants are less dramatic, although there is an increase (6 Å) in the distance between positions 246 and 261 and a decrease (8 Å) between positions 137 and 261.

Fourth, the ATP-bound state of TRiC was mimicked by adding the nonhydrolyzable ATP analogue, AMP-PNP, to the β-actin^{cys+}−TRiC/ADP complex. It is known that ATP-binding results in conformational changes in TRiC, in particular in the apical domains where the actin molecule is proposed to bind (*41*). The homo-FRET measurements clearly show that these nucleotide-dependent conformational changes in the chaperonin drastically affect the conformation of the bound actin molecule. This is in particular obvious for the distance between positions 39 and 246, where a dramatic decrease ($\geq$33 Å) occurs. Note also that the distance between positions 86 and 261 is shortened by 7 Å, while the distances between 246 and 261 and 137 and 261 are more or less unchanged.

Intact Chaperonin Function Is Shown by Substrate Release That Is Dependent upon ATP Hydrolysis. To verify the proper function of TRiC, it is important to show that β-actin^{cys+} can not only bind to the chaperonin but also be released from the cavity. Because anisotropy is dependent upon the size of the labeled molecule, the release of a β-actin^{cys+} monomer with a molecular weight of about 42 kDa would cause a major drop in anisotropy compared to when it is bound to the 900 kDa complex of the chaperonin TRiC. However, non-native actin could aggregate as it is released from the chaperonin cavity into the surrounding buffer. Furthermore, released native actin monomers can polymerize, leading to larger complexes. In both of these cases, the anisotropy values could (by chance) resemble those of actin bound to TRiC. Interestingly, DNase I binds to a loop in subdomain 2 of native, monomeric actin (Figure 1), thereby preventing actin polymerization into fibrous actin. DNase I can only form a high-affinity complex with full-length and correctly folded actin (*42*, *43*).

Here, we performed an experiment in which DNase I was added to the solution containing the β-actin^{cys+}−TRiC/ADP complex before subsequent addition of ATP. We show that TRiC has a retained proper function in our *in vitro* experiments; ATP hydrolysis leads to the release of the bound Q137C, L261C, and Q137C/L261C variants from TRiC. The release is shown by a significant drop in anisotropy (shown for L261C in Figure 3F), which is due to the faster tumbling of the DNase-I-bound β-actin^{cys+} molecule after release from the larger TRiC complex.

The anisotropy of the proposed actin−DNase I complex is higher than that for β-actin^{cys+} dissolved in 4 M GuHCl but lower than that for β-actin^{cys+} diluted into folding buffer with no chaperonin present, where aggregates of non-native β-actin^{cys+} are formed upon storage (Figure 3F). Our interpretation of these anisotropy values is that β-actin^{cys+} Q137C, L261C, and Q137C/L261C adopts a native or close to native structure after one chaperonin cycle with the subsequent release. For the other β-actin^{cys+} variants, we observed a significant drop in anisotropy (data not shown), but the anisotropies in those cases were more similar to the anisotropy of the β-actin^{cys+} aggregates, which are formed when diluting β-actin^{cys+} from 4 M GuHCl to folding buffer. Considering all of the mutations and insertion of probes in the β-actin^{cys+} molecule, it is not surprising if not all of our investigated β-actin^{cys+} variants can reach the native state. However, they all bind to TRiC and show a coherent pattern of conformational rearrangements as a result of nucleotide-dependent rearrangements of the TRiC molecule. Thus, the rearrangement of the TRiC complex forces the bound β-actin^{cys+} molecule to rearrange into a conformation that is

competent to fold to the native state upon release from TRiC after ATP hydrolysis.

DISCUSSION

FRET is a sensitive method for studying protein−protein interactions and dynamics and can be used to study relative distance changes in a well-defined system. Here, it is applied to examine the mechanism of the TRiC chaperonin when assisting the folding of its prime target protein actin. TRiC and actin in the studied system are identical to the proteins found in bovine cells. Interestingly, the bovine TRiC amino acid sequence differs only by ∼3% from the human counterpart, and the actin amino acid sequence is identical in cows and humans. Thus, the actin−TRiC interactions studied in the bovine system would probably be similar to the interactions in human cells. The actin template used in our work was designed without the native cysteine residues, abbreviated β-actin^{cys-}. This rendered the molecule prone to misfold and aggregate. This is important because it enables efficient capture of the actin substrate protein. It has been shown that actin binds to both GroEL and TRiC but is only chaperoned into the native product by TRiC (*44*). However, the binding seemed to be weaker to TRiC than to GroEL. Importantly, the use of the β-actin^{cys+} variants, in the present study, enabled efficient capture by TRiC, when TRiC was used in 4-fold excess over β-actin^{cys+}. The variant β-actin^{cys+} hence can resemble the highly homologous cardiac α-actin disease-associated mutants believed to cause hypertrophic and dilated cardiomyopathy (*45*), several of which have been shown to populate partially folded states (*43*). More interestingly, especially the mutant R312H showed prolonged binding to TRiC during *in vitro* biosynthesis and folding (*43*). We were intrigued by the possibility of being able to monitor the conformational changes of a captured actin molecule in the TRiC chaperonin by FRET.

The sites for attachment of fluorescein were chosen after inspection based on the known native structure of β-actin (*46*). The actin molecule is divided by the nucleotide-binding cleft into a small and a large domain. Each domain is further divided into two subdomains, with the small domain consisting of subdomains 1 and 2 and the large domain consisting of subdomains 3 and 4 (Figure 1). To analyze rearrangements between the four subdomains, the positions chosen for fluorescein labeling are spread throughout the structure. Orientational differences of the fluorescein labels can add uncertainties to the distance calculations, especially if such movements at both sites occur in concert. Using 4 pairs of labeled sites to obtain a medium resolution distance map of the bound actin molecule, we aimed to minimize the risk that our interpretations were skewed by local reorientations of the fluorescein side chains. As can be seen in Table 1, several of the changes in the distance are much larger than can be explained by mere reorientation of the fluorophores. The actin variant R39C/Q246C was chosen because of results from cryo-EM experiments (*6*), which indicate large nucleotide-dependent rearrangements in relative positions of subdomains 2 and 4 upon the interaction with TRiC. The Q246C/L261C variant was chosen to report on events within a defined subdomain (subdomain 4), and the variants W86C/L261C and Q137C/L261C were chosen to report on rearrangements that might occur between subdomains 4 and 1. To maximize the chance to monitor changes in the distance upon the interaction with TRiC, the distances between the attachment sites for the fluorophores all lay in the 20−40 Å range in the native actin molecule.

In the following sections, we will discuss the rearrangements of the actin subdomains in detail, as the solvent and conditions for the interaction with TRiC are altered. We describe how the actin structure is affected when non-native actin [a distinct intermediate I_3 according to Altschuler et al. (*47*)] rearranges upon binding to the cavity of the TRiC/ADP complex and how binding of the ATP analogue, AMP-PNP, to TRiC causes conformational changes in the bound actin molecule.

The distances were mainly obtained from the effects of FRET on the fluorescence anisotropy that is determined in steady-state measurements. In addition, the reliability of these values was demonstrated by the very similar distance values that were obtained from both time-resolved and steady-state anisotropy measurements on actin variants dissolved in 7.5 M GuHCl.

Binding to TRiC/ADP Leads to Forced Rearrangements of the Target Protein. To examine how actin is affected upon binding to TRiC, the denaturated labeled actin was diluted 125−300-fold from 4 M GuHCl into a folding solution containing TRiC/ADP. This results in a final GuHCl concentration of 12−32 mM. At this low GuHCl concentration, TRiC is stable and active, according to earlier folding assays of actin in complex with TRiC, where a GuHCl concentration of 60 mM did not affect the folding negatively (*2*, *48*). To minimize aggregation and maximize the degree of actin binding to TRiC, the final molar concentration of the TRiC/ADP complex was 4 times higher than the actin concentration. Moreover, the total protein concentrations were kept low (0.4 μM actin and 1.6 μM TRiC) to further minimize the risk of aggregation. Notably, Chik et al. (*47*) have shown that a stable unfolding intermediate (I_3) of actin, which may well be the natural substrate for TRiC, does not aggregate at these low concentrations. In summary, the conditions used seem to be beneficial for productive interactions between actin and TRiC.

β-actin^{cys+} was also diluted in the same way from 4 M GuHCl into folding buffer without any TRiC/ADP present, leading to non-native actin molecules with a tendency to aggregate. The distances in all double variants were measured, and the results (Table 1) implicate that the actin molecule becomes, overall, more compact in 0 M GuHCl. However, the aggregated states of non-native actin in 0 M GuHCl are not well-characterized, and instead, the unfolded state of actin in 4 M GuHCl is used as a reference in the distance comparisons between unfolded actin and actin bound to TRiC/ADP. The 0 M GuHCl measurements are important, though, to emphasize that the contribution from any possible remaining non-native actin molecules or aggregates in the actin−TRiC/ADP measurements is negligible. Notably, a comparison with the observed distance at 0 M GuHCl indicates that the active stretching upon binding to the chaperonin may increase the distance between positions 39 and 246 by more than 22 Å.

As non-native actin binds to TRiC/ADP, the 39−246 distance is increased by ≥12 Å; thus, the subdomains 2 and 4 are forced to move apart (parts B and C of Figure 5 and Table 1). The cryo-EM structure from Llorca and co-workers (*6*) shows that actin interacts with two of the subunits in

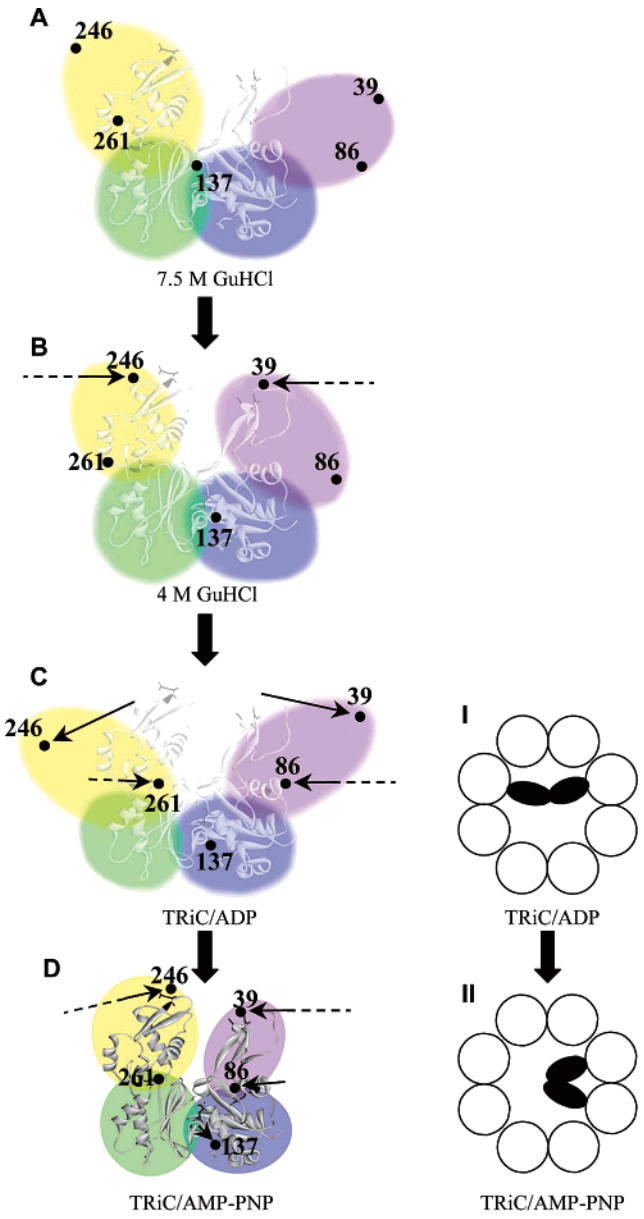

FIGURE 5: Rearrangements in the actin molecule. (A−D) Schematic representation of the rearrangements in the actin molecule upon stepwise transfer from highly denaturing conditions to the interaction with TRiC/ADP and TRiC/AMP-PNP. The colored areas represent subdomain 1 (blue), subdomain 2 (pink), subdomain 3 (green), and subdomain 4 (yellow) of the actin molecule. The ribbon representation of native β-actin from Figure 1 is superimposed onto the colored areas to emphasize the rearrangements of the actin subdomains as the conditions are altered. Arrows at the labeled positions indicate major directional changes that have occurred in the process leading to this state. Dashed arrows represent changes where the starting distance between the labeled positions could not be determined (>55 Å in GuHCl or >68 Å in TRiC). Arrows with a continuous line represent changes where the starting distance between the labeled positions is known. I and II are schematic representations of the TRiC−actin complex as measured by cryo-EM (*6*).

TRiC sitting in the 1−4 position relative to each other (almost opposite each other) and that the upper parts of subdomains 2 and 4 make these interactions (Figure 5). This leaves the actin molecule in an "open" configuration, which corresponds well with the >68 Å distance shown by the homo-FRET measurements. In addition to this large increase in distance between the subdomains 2 and 4, we also see stretching in subdomain 4, as indicated by the 6 Å increase between positions 246 and 261.

Another striking change is the ≥10 Å shortening of the distance between positions 86 and 261. Thus, the unstructured and flexible parts of the molecule, present in 4 M GuHCl, seem to have disappeared, and actin becomes more compact in this region when bound to TRiC/ADP. The distance between 137 and 261 is also shortened (by 8 Å), which indicates that subdomain 3 becomes more compact. This increased compactness in some parts of the actin molecule is gained passively through the removal of the denaturant or actively by binding to the chaperonin, which is not possible to deduce from our data.

Stretching Is Relieved by ATP (AMP-PNP) Binding to the Chaperonin. The next step in the chaperonin mechanism *in vivo* would be ATP binding to the equatorial domains of each chaperonin subunit in the octameric ring to which actin is attached. Earlier studies have shown that ATP binding to the equatorial domains of TRiC induces conformational changes that are transmitted from the equatorial domain through the intermediate domain to the apical domain, leading to the closure of the cavity by a 70° twist of the helical protrusions in the tips of the apical domains (*7*, *49*). Recall that ATP binding solely induces conformational changes but does not release the target protein because the release is dependent upon ATP hydrolysis (*6*).

In the present study, the ATP-bound state of TRiC was mimicked by adding the nonhydrolyzable ATP analogue, AMP-PNP, in 100-fold molar excess compared to TRiC. Again, homo-FRET measurements report on large rearrangements within the actin molecule (Figure 5). Positions 39 and 246 in subdomains 2 and 4 are brought closer together (by ≥33 Å), and the 86−261 distance continues to decrease, by 7 Å, while there might be a small increase between 137 and 261 (3 Å; Table 1). Overall, the actin molecule is forced into a more compact state by the twist of the apical domains of TRiC, indicating a compression of the TRiC-bound actin during AMP-PMP binding. These results are also in accordance with the cryo-EM pictures published by Llorca et al. (*6*; I and II in the right panel of Figure 5). From a comparison of the distances obtained from the homo-FRET measurements to the distances between the β carbons of the labeled amino acid residues in the native structure, it is obvious that the compactness of actin in the TRiC/AMP-PNP−actin complex is close to that of subdomains 2 and 4 in native actin (Table 1). The FRET-derived distances in R39C/Q246C and W86C/L261C are remarkably similar to the distances in native actin. The observed distances for Q246C/L261C and Q137C/L261C are longer in the TRiC/AMP-PNP−actin complex than in native actin. These observation either indicate that these regions become more structured upon the release from TRiC or indicate that that the fluorescein molecules, which can add approximately 6 Å to the distance, could point in opposite directions in the TRiC/AMP-PNP−actin complex, thus reporting a larger distance than the true distance between the β carbons.

Notably, inspection of the anisotropies for the singly labeled variants shows that actin single variants R39C, W86C, Q246C, and L261C have essentially the same anisotropy in TRiC/ADP and TRiC/AMP-PNP complexes (parts B−E of Figure 3). Because the anisotropy is dependent upon both the size of the complex (speed of tumbling) and

the local rotation of the fluorescein label, these results support earlier reports that ATP binding alone does not result in the release of a bound target protein (*6*) and that the fluorophore in these variants experiences very similar environments in complex with TRiC/ADP and TRiC/AMP-PNP. However, at position 137, the anisotropy decreases considerably upon the addition of AMP-PNP (Figure 3D), indicating that position 137 is more flexible in actin bound to TRiC/AMP-PNP than in actin bound to TRiC/ADP. Note that this observation supports the FRET results by showing that binding of ATP (AMP-PNP) leads to conformational rearrangements in the hinge region around position 137.

Release of actin from TRiC only occurs following ATP addition (not AMP-PNP binding), indicating that the hydrolysis of ATP is a requirement for release (Figure 3F).

CONCLUSIONS

In simple organisms, GroEL-type chaperonins display a symmetric arrangement of homo-oligomeric ring structures, whereas in more advanced species, hetero-oligomeric chaperonins have evolved, likely to interact in a more specific manner with a variety of substrates. Chaperonins are designed for multiple-valence binding of substrate proteins to the apical domains. This multiple-valence binding is well-suited to interact with partially folded globular proteins. In this paper, we have employed fluorescein homo-FRET to study the structural dynamics of actin bound to the chaperonin TRiC, a natural pair of protein substrate−chaperone found in all eukaryotic cells. Further, we used GuHCl denaturation as a comparative measure of the compactness of actin as a reference to the structural rearrangements invoked by TRiC. Actin unfolded by 4 M GuHCl displays a rather compact unfolded state, which, during 125−300-fold dilution into the TRiC-containing folding buffer, is likely to collapse even more. Nevertheless, the TRiC-bound actin displays a stretched structure showing extended distances close to unfolded actin in 7.5 M GuHCl, showing that binding to TRiC forces the actin molecule away from a compact state into an elongated state. This forced rearrangement is completely ATP-independent and is likely facilitated through efficient utilization of the binding energy between the TRiC and actin to induce an energetically more favorable interaction surface. Upon AMP-PMP binding, the conformational change in the TRiC chaperonin allows the actin molecule to relax into a compact state. This rearrangement may occur spontaneously or through active compression. Thus, the actin molecule is affected by TRiC (through stretching and compaction) in ways strikingly reminiscent of the GroEL substrate protein interactions that we and others have reported previously. We conclude that the mechanism for assisted folding by chaperonins is evolutionary-conserved and can be summarized in three steps: (i) ATP-independent active stretching of partially folded globular substrates through the use of binding energy, (ii) promotion of correct folding by ATP (AMP-PNP) binding, which relieves the stretching of the substrate, and (iii) ATP hydrolysis to release the substrate from the chaperonin.

SUPPORTING INFORMATION AVAILABLE

Detailed procedures for purifying TRiC, theory on steady-state and time-resolved homo-FRET, and a table presenting dynamic parameters of the five single variants in 7.5 M GuHCl obtained by deconvolution fitting. This material is available free of charge via the Internet at http://pubs.acs.org.

REFERENCES

1. Lewis, V. A., Hynes, G. M., Zheng, D., Saibil, H., and Willison, K. (1992) T-complex polypeptide-1 is a subunit of a heteromeric particle in the eukaryotic cytosol, *Nature 358*, 249−252.
2. Frydman, J., Nimmesgern, E., Erdjument-Bromage, H., Wall, J. S., Tempst, P., and Hartl, F.-U. (1992) Function in protein folding of TRiC, a cytosolic ring complex containing TCP-1 and structurally related subunits, *EMBO J. 11*, 4767−4778.
3. Rommelaere, H., Van Troys, M., Gao, Y., Melki, R., Cowan, N. J., Vandekerckhove, J., and Ampe, C. (1993) Eukaryotic cytosolic chaperonin contains t-complex polypeptide 1 and seven related subunits, *Proc. Natl. Acad. Sci. U.S.A. 90*, 11975−11979.
4. Kubota, H., Hynes, G., Carne, A., Ashworth, A., and Willison, K. (1994) Identification of six Tcp-1-related genes encoding divergent subunits of the TCP-1-contatining chaperonin, *Curr. Biol. 4*, 89−99.
5. Pappenberger, G., Wilsher, J. A., Roe, S. M., Counsell, D. J., Willison, K. R., and Pearl, L. H. (2002) Crystal structure of the CCT apical domain: Implications for substrate binding to the eukaryotic cytosolic chaperonin, *J. Mol. Biol. 318*, 1367−1379.
6. Llorca, O., Martín-Benito, J., Grantham, J., Ritco-Vonsovici, M., Willison, K. R., Carrascosa, J. L., and Valpuesta, J. M. (2001) The "sequential allosteric ring" mechanism in the eukaryotic chaperonin-assisted folding of actin and tubulin, *EMBO J. 20*, 4065−4075.
7. Llorca, O., Smyth, M. G., Carrascosa, J. L., Willison, K. R., Radermacher, M., Steinbacher, S., and Valpuesta, J. M. (1999) 3D reconstruction of the ATP-bound form of CCT reveals the asymmetric folding conformation of a type II chaperonin, *Nat. Struct. Biol. 6*, 639−642.
8. Kafri, G., and Horovitz, A. (2003) Transient kinetic analysis of ATP-induced allosteric transitions in the eukaryotic chaperonin containing TCP-1, *J. Mol. Biol. 326*, 981−987.
9. Chen, X., Sullivan, D. S., and Huffaker, T. C. (1994) Two yeast genes with similarity to TCP-1 are required for microtubule and actin function in vivo, *Proc. Natl. Acad. Sci. U.S.A. 91*, 9111−9115.
10. Spiess, C., Meyer, A. S., Reissmann, S., and Frydman, J. (2004) Mechanism of the eukaryotic chaperonin: Protein folding in the chamber of secrets, *Trends Cell Biol. 14*, 598−604.
11. Thulisiraman, V., Yang, C.-F., and Frydman, J. (1999) *In vivo* newly translated polypeptides are sequestered in a protected folding environment, *EMBO J. 18*, 85−95.
12. Tian, G., Vainberg, I. E., Tap, W. D., Lewis, S. A., and Cowan, N. J. (1995) Quasi-native chaperonin-bound intermediates in facilitated protein folding, *J. Biol. Chem. 270*, 23910−23913.
13. Melki, R., and Cowan, N. J. (1994) Facilitated folding of actins and tubulins occurs via a nucleotide-dependent interaction between cytoplasmic chaperonin and distinctive folding intermediates, *Mol. Cell. Biol. 14*, 2895−2904.
14. Lewis, S. A., Tian, G., Vainberg, I. E., and Cowan, N. J. (1996) Chaperonin-mediated folding of actin and tubulin, *J. Cell Biol. 132*, 1−4.
15. Dobrzynski, J. K., Sternlicht, M. L., Farr, G. W., and Sternlicht, H. (1996) Newly-synthesized β-tubulin demonstrates domain-specific interactions with the cytosolic chaperonin, *Biochemistry 35*, 15870−15882.
16. Ellis, R. J. (1996) Revisiting the Anfinsen cage, *Folding Des. 1*, R9−R15.
17. Todd, M. J., Lorimer, G. H., and Thirumalai, D. (1996) Chaperonin-facilitated protein folding: Optimization of rate and yield by an iterative annealing mechanism, *Proc. Natl. Acad. Sci. U.S.A. 93*, 4030−4035.
18. Todd, M. J., Viitanen, P. V., and Lorimer, G. H. (1994) Dynamics of the chaperonin ATPase cycle: Implications for facilitated protein folding, *Science 265*, 659−666.
19. Weissman, J. S., Kashi, Y., Fenton, W. A., and Horwich, A. L. (1994) GroEL-mediated protein folding proceeds by multiple rounds of binding and release of nonnative forms, *Cell 78*, 693−702.
20. Smith, K. E., and Fisher, M. T. (1995) Interactions between the GroE chaperonins and rhodanese. Multiple intermediates and release and rebinding, *J. Biol. Chem. 270*, 21517−21523.

21. Taguchi, H., and Yoshida, M. (1995) Chaperonin releases the substrate protein in a form with tendency to aggregate and ability to rebind to chaperonin, *FEBS Lett. 359*, 195−198.
22. Burston, S. G., Weissman, J. S., Farr, G. W., Fenton, W. A., and Horwich, A. L. (1996) Release of both native and non-native proteins from a cis-only GroEL ternary complex, *Nature 383*, 96−99.
23. Sparrer, H., Lilie, H., and Buchner, J. (1996) Dynamics of the GroEL−protein complex: Effects of nucleotides and folding mutants, *J. Mol. Biol. 258*, 74−87.
24. Shtilerman, M., Lorimer, G. H., and Englander, S. W. (1999) Chaperonin function: Folding by forced unfolding, *Science 284*, 822−825.
25. Park, E. S., Fenton, W. A., and Horwich, A. L. (2005) No evidence for a forced-unfolding mechanism during ATP/GroES binding to substrate-bound GroEL: No observable protection of metastable Rubisco intermediate or GroEL-bound Rubisco from tritium exchange, *FEBS Lett. 579*, 1183−1186.
26. Lin, Z., and Rye, H. (2004) Expansion and compression of a protein folding intermediate by GroEL, *Mol. Cell 16*, 23−34.
27. Persson, M., Hammarstrom, P., Lindgren, M., Jonsson, B. H., Svensson, M., and Carlsson, U. (1999) EPR mapping of interactions between spin-labeled variants of human carbonic anhydrase II and GroEL: Evidence for increased flexibility of the hydrophobic core by the interaction, *Biochemistry 38*, 432−441.
28. Hammarström, P., Persson, M., and Carlsson, U. (2001) Protein compactness measured by fluorescence resonance energy transfer. Human carbonic anhydrase II is considerably expanded by the interaction of GroEL, *J. Biol. Chem. 276*, 21765−21775.
29. Hammarström, P., Persson, M., Owenius, R., Lindgren, M., and Carlsson, U. (2000) Protein substrate binding induces conformational changes in the chaperonin GroEL. A suggested mechanism for unfoldase activity, *J. Biol. Chem. 275*, 22832−22838.
30. Persson, M., Aronsson, G., Bergenhem, N., Freskgard, P. O., Jonsson, B. H., Surin, B. P., Spangfort, M. D., and Carlsson, U. (1995) GroEL/ES-mediated refolding of human carbonic anhydrase II: Role of N-terminal helices as recognition motifs for GroEL, *Biochim. Biophys. Acta 1247*, 195−200.
31. Persson, M., Carlsson, U., and Bergenhem, N. (1997) GroEL provides a folding pathway with lower apparent activation energy compared to spontaneous refolding of human carbonic anhydrase, *FEBS Lett. 411*, 43−47.
32. Kost, T. A., Theodorakis, N., and Hughes, S. H. (1983) The nucleotide sequence of the chick cytoplasmic β-actin gene, *Nucleic Acids Res. 11*, 8287−8301.
33. Weber-Nielsen, M., Vandehaar, M. J., Xiao, L., Tempelman, R. J., and Coussens, P. M. (2003) Bovine mammary gene expression profiling using a cDNA microarray enhanced for mammary-specific transcripts, *Physiol. Genomics 16*, 8−18.
34. Nair, S. K., Calderone, T. L., Christianson, D. W., and Fierke, C. A. (1991) Altering the mouth of a hydrophobic pocket. Structure and kinetics of human carbonic anhydrase II mutants at residue Val-121, *J. Biol. Chem. 266*, 17320−17325.
35. Schüler, H., Korenbaum, E., Schutt, C. E., Lindberg, U., and Karlsson, R. (1999) Mutational analysis of Ser14 and Asp157 in the nucleotide-binding site of β-actin, *Eur. J. Biochem. 265*, 210−220.
36. Riddles, P. W., Blakely, R. L., and Zerner, B. (1983) Reassessment of Ellman's reagent, *Methods Enzymol. 91*, 49−60.
37. Ferreyra, R., and Frydman, J. (2000) Purification of the cytosolic chaperonin TRiC from bovine testis, in *Chaperonin Protocols* (Schneider, C., Ed.) pp 153−160, Humana Press, Totowa, NJ.
38. Lakowicz, J. R. (1999) *Principles of Fluorescence Spectroscopy*, Kluwer Academic/Plenum Publishers, New York.
39. Hamman, B. D., Oleinikov, A. V., Jokhadze, G. G., Traut, R. R., and Jameson, D. M. (1996) Dimer/monomer equilibrium and domain separations of *Escherichia coli* ribosomal protein L7/L12, *Biochemistry 35*, 16680−16686.
40. Sternlicht, H., Farr, G. W., Sternlicht, M. L., Driscoll, J. K., Willison, K., and Yaffe, M. B. (1993) The t-complex polypeptide 1 complex is a chaperonin for tubulin and actin in vivo, *Proc. Natl. Acad. Sci. U.S.A. 90*, 9422−9426.
41. Llorca, O., McCormack, E., Hynes, G., Grantham, J., Cordell, J., Carrascosa, J. L., Willison, K. R., Fernández, J. J., and Valpuesta, J. M. (1999) Eukaryotic type II chaperonin CCT interacts with actin through specific subunits, *Nature 402*, 693−696.
42. Schüler, H., Lindberg, U., Schutt, C. E., and Karlsson, R. (2000) Thermal unfolding of G-actin monitored with the DNase I-inhibition assay, *Eur. J. Biochem. 267*, 476−486.
43. Vang, S., Corydon, T. J., Borglum, A. D., Scott, M. D., Frydman, J., Mogensen, J., Gregersen, N., and Bross, P. (2005) Actin mutations in hypertrophic and silated cardiomyopathy cause inefficient protein folding and pertubed filament formation, *FEBS J. 272*, 2037−2049.
44. Tian, G., Vainberg, I. E., Tap, W. D., Lewis, S. A., and Cowan, N. J. (1995) Specificity in chaperonin-mediated protein folding, *Nature 375*, 250−253.
45. Olson, T. M., Michels, V. V., Thibodeau, S. N., Tai, Y.-S., and Keating, M. T. (1998) Actin mutations in dilated cardiomyopathy, a heritable form of heart failure, *Science 280*, 750−752.
46. Chik, J. K., Lindberg, U., and Schutt, C. E. (1996) The structure of an open state of β-actin at 2.65 Å resolution, *J. Mol. Biol. 263*, 607−623.
47. Altschuler, G. M., Klug, D. R., and Willison, K. (2005) Unfolding energetics of G-α-actin: A discrete intermediate can be re-folded to the native state by CCT, *J. Mol. Biol. 353*, 385−396.
48. Gao, Y., Thomas, J. O., Chow, R. L., Lee, G.-H., and Cowan, N. J. (1992) A cytoplasmic chaperonin that catalyzes β-actin folding, *Cell 69*, 1043−1050.
49. Nitsch, M., Walz, J., Typke, D., Klumpp, M., Essen, L. O., and Baumeister, W. (1998) Group II chaperonin in an open conformation examined by electron tomography, *Nat. Struct. Biol. 5*, 855−857.

BI062093O